LISA Pathfinder micronewton cold gas thrusters: In-flight characterization

M. Armano,[1] H. Audley,[2] J. Baird,[3] P. Binetruy,[3,*] M. Born,[2] D. Bortoluzzi,[4] E. Castelli,[5] A. Cavalleri,[6] A. Cesarini,[7] A. M. Cruise,[8] K. Danzmann,[2] M. de Deus Silva,[9] I. Diepholz,[2] G. Dixon,[8] R. Dolesi,[5] L. Ferraioli,[10] V. Ferroni,[5] E. D. Fitzsimons,[11] M. Freschi,[9] L. Gesa,[12] F. Gibert,[5] D. Giardini,[10] R. Giusteri,[5] C. Grimani,[7] J. Grzymisch,[1] I. Harrison,[13] G. Heinzel,[2] M. Hewitson,[2] D. Hollington,[14] D. Hoyland,[8] M. Hueller,[5] H. Inchauspé,[3,15] O. Jennrich,[1] P. Jetzer,[16] N. Karnesis,[3] B. Kaune,[2] N. Korsakova,[17] C. J. Killow,[17] J. A. Lobo,[12,†] I. Lloro,[12] L. Liu,[5] J. P. López-Zaragoza,[12] R. Maarschalkerweerd,[13] D. Mance,[10] N. Meshksar,[10] V. Martín,[12] L. Martin-Polo,[9] J. Martino,[3,‡] F. Martin-Porqueras,[9] I. Mateos,[12] P. W. McNamara,[1] J. Mendes,[13] L. Mendes,[9] M. Nofrarias,[12] S. Paczkowski,[2] M. Perreur-Lloyd,[17] A. Petiteau,[3] P. Pivato,[5] E. Plagnol,[3] J. Ramos-Castro,[18] J. Reiche,[2] D. I. Robertson,[17] F. Rivas,[12] G. Russano,[5] J. Slutsky,[19] C. F. Sopuerta,[12] T. Sumner,[14] D. Texier,[9] J. I. Thorpe,[19] D. Vetrugno,[5] S. Vitale,[5] G. Wanner,[2] H. Ward,[17] P. J. Wass,[14,15] W. J. Weber,[5] L. Wissel,[2] A. Wittchen,[2] and P. Zweifel[10]

(LISA Pathfinder Collaboration)

[1]*European Space Technology Centre, European Space Agency, Keplerlaan 1, 2200 AG Noordwijk, Netherlands*
[2]*Albert-Einstein-Institut, Max-Planck-Institut für Gravitationsphysik und Leibniz Universität Hannover, Callinstraße 38, 30167 Hannover, Germany*
[3]*APC, Univ Paris Diderot, CNRS/IN2P3, CEA/lrfu, Obs de Paris, Sorbonne Paris Cité, France*
[4]*Department of Industrial Engineering, University of Trento, via Sommarive 9, 38123 Trento, and Trento Institute for Fundamental Physics and Application / INFN*
[5]*Dipartimento di Fisica, Università di Trento and Trento Institute for Fundamental Physics and Application/INFN, 38123 Povo, Trento, Italy*
[6]*Istituto di Fotonica e Nanotecnologie, CNR-Fondazione Bruno Kessler, I-38123 Povo, Trento, Italy*
[7]*DISPEA, Università di Urbino "Carlo Bo", Via S. Chiara, 27 61029 Urbino/INFN, Italy*
[8]*The School of Physics and Astronomy, University of Birmingham, Birmingham, United Kingdom*
[9]*European Space Astronomy Centre, European Space Agency, Villanueva de la Cañada, 28692 Madrid, Spain*
[10]*Institut für Geophysik, ETH Zürich, Sonneggstrasse 5, CH-8092, Zürich, Switzerland*
[11]*The UK Astronomy Technology Centre, Royal Observatory, Edinburgh, Blackford Hill, Edinburgh, EH9 3HJ, United Kingdom*
[12]*Institut de Ciències de l'Espai (CSIC-IEEC), Campus UAB, Carrer de Can Magrans s/n, 08193 Cerdanyola del Vallès, Spain*
[13]*European Space Operations Centre, European Space Agency, 64293 Darmstadt, Germany*
[14]*High Energy Physics Group, Physics Department, Imperial College London, Blackett Laboratory, Prince Consort Road, London, SW7 2BW, United Kingdom*
[15]*Department of Mechanical and Aerospace Engineering, MAE-A, P.O. Box 116250, University of Florida, Gainesville, Florida 32611, USA*
[16]*Physik Institut, Universität Zürich, Winterthurerstrasse 190, CH-8057 Zürich, Switzerland*
[17]*SUPA, Institute for Gravitational Research, School of Physics and Astronomy, University of Glasgow, Glasgow, G12 8QQ, United Kingdom*
[18]*Department d'Enginyeria Electrònica, Universitat Politècnica de Catalunya, 08034 Barcelona, Spain*
[19]*Gravitational Astrophysics Lab, NASA Goddard Space Flight Center, 8800 Greenbelt Road, Greenbelt, Maryland 20771, USA*

(Received 29 April 2019; published 28 June 2019)

The LISA Pathfinder (LPF) mission has demonstrated the ability to limit and measure the fluctuations in acceleration between two free falling test masses down to sub-femto-g levels. One of the key elements to achieve such a level of residual acceleration is the drag free control. In this scheme the spacecraft is used as a shield against any external disturbances by adjusting its relative position to a reference test mass.

[*]Deceased 30 March 2017.
[†]Deceased 30 September 2012.
[‡]martino@apc.in2p3.fr

The actuators used to move the spacecraft are cold gas micropropulsion thrusters. In this paper, we report in-flight characterization of these thrusters in term of noise and artefacts during science operations using all the metrology capabilities of LISA Pathfinder. Using the LISA Pathfinder test masses as an inertial reference frame, an average thruster noise of ∼0.17 μN/Hz is observed and decomposed into a common (coherent) and an uncorrelated component. The very low noise and stability of the onboard metrology system associated with the quietness of the space environment allowed the measurement of the thruster noise down to ∼20 μHz, more than an order of magnitude below any ground measurement. Spectral lines were observed around ∼1.5 mHz and its harmonics and around 55 and 70 mHz. They are associated with the cold gas system itself and possibly to a clock synchronization issue. The thruster noise-floor exhibits an excess of ∼70% compared to characterization that have been made on ground on a single unit and without the feeding system. However this small excess has no impact on the LPF mission performance and is compatible with the noise budget for the upcoming LISA gravitational wave observatory. Over the whole mission, nominal, and extension, the thrusters showed remarkable stability for both the science operations and the different maneuvers necessary to maintain LPF on its orbit around L1. It is therefore concluded that a similar cold gas system would be a viable propulsion system for the future LISA mission.

DOI: 10.1103/PhysRevD.99.122003

I. INTRODUCTION

LISA Pathfinder (LPF) was a European Space Agency mission [1] that demonstrated several technical milestones for the future gravitational wave observatory LISA [2]. In order to do so, two test masses (TM) of 1.92 kg and separated by 37 cm were placed in free fall at a level of differential acceleration of 1.74 $\mathrm{fm\,s^{-2}}/\sqrt{\mathrm{Hz}}$ down to a mHz [3]. One of the hardware components on which this performance relies is the *cold gas* micropropulsion system [4–6]. LISA Pathfinder has a total of 12 cold gas microthrusters divided in two similar sets, prime and redundant, of 6 thrusters. Only one set can be used at the time.

In the low noise space environment, perturbations like solar wind, micrometeorites or simply the self-gravity of the satellite can strongly impact the performances. To prevent these perturbations from disturbing the test masses, the relative positions between the spacecraft (SC) and one of the free floating TMs is constantly monitored and maintained constant by adjusting the SC position using the thruster system. This strategy that forces the spacecraft to follow the test masses is called drag free and is implemented by the Drag Free and Attitude Control System (*DFACS*)[7]. The required range capability of the thrusters is directly dictated by the expected DC forces and torques on the spacecraft. During science operations for instance, the solar pressure plus the outgoing infrared radiation from the spacecraft, the sum estimated at around 25 μN, is the main contributor in term of DC force. This value was calculated along a direction perpendicular to the solar panel assuming a perfect pointing of the solar panels toward the sun. Six thrusters are used at the same time, consequently the mean thrusts required per thrusters by taking into account their orientation, see Table I, is around 9 μN.

This is for the static disturbances, but frequency dependent TM/SC motion have also to be nulled-out by the drag free loop up to 100 mHz. In any standard mission the noise coming from the micropropulsion system will result in the jittering of the spacecraft. In LPF this jittering is strongly attenuated by the drag free loop as the commanded thrusts will mirror their own noise with a 180 degrees phase shift. Nevertheless some relative motion is still present due to the thruster noise. While the main measurement in LPF or in a gravitational wave observatory like LISA are accelerations between the free-falling test masses, motion of the surrounding spacecraft can introduce both measurement errors from cross-talk and dynamical coupling from force gradients [8]. In order to satisfy the expected performance of LPF, the requirement on the control accuracy of the S/C motion along the sensitive axis between 1 mHz and 30 mHz was 2.5 nm/Hz. That sets the level for each thruster noise at 0.1 μN/Hz giving LPF's drag free controller design.

The cold gas propulsion system is also used for different maneuvers that are not directly related to the science operations such as weekly *station keeping* to maintain the orbit around L1 (where TMs were kept in place electromagnetically) or spinning and despinning during the spacecraft/propulsion module separation (where TMs were still grabbed). These phases required to operate the thrusters at higher thrusts, up to 500 μN and with different

TABLE I. Thruster direction cosines.

Thruster direction cosines			
Thruster	X	Y	Z
1	−0.078310	−0.864364	0.496732
2	−0.787716	0.364364	0.496732
3	0.787716	0.364364	0.496732
4	0.078310	−0.864364	0.496732
5	−0.709406	0.500000	0.496732
6	0.709406	0.500000	0.496732

requirements. The performance and characterization during those phases are beyond the scope of this paper. Outside of these periods, the satellite was kept in *science operation* mode. Most of the results shown in this study come from special science periods when the satellite is in a *noise-only* state, i.e., when forces applied to the spacecraft or the test masses are only those necessary to keep it in drag free and attitude control mode. In the following, the data are referenced by the Day of the Year (*DoY*) measuring the number of days from the first of January 2016. LISA Pathfinder was launched on the 4th of December 2015 and was in *commission mode* during the month of February 2016. Science operations started on the 1st of March 2016. The mission was ended in July 2017.

In Sec. II, an overview of the thrusters hardware setup and in particular the gas feeding system is presented. Section III will describe the in-flights characterization of the cold gas in term of noise and anomalies. In Sec. IV potential consequences for LISA are presented and in Sec. V some conclusions are given.

II. COLD GAS MICRONEWTON HARDWARE

Each thruster can be described with four main parts represented in Fig. 1:

(i) A mass flow sensor: the flow is proportional to the level of thrust.
(ii) A piezo valve that controls the flow according to the requested thrust.
(iii) A micro-propulsion electronics unit (MPE) common to the six thrusters.
(iv) The nitrogen feeding system, common to the six thrusters.

The MPE runs an internal closed loop at 40 Hz that commands the aperture of the valve. This command is proportional to the error between the requested thrusts sent by the on-board computer at 10 Hz and the measured thrusts computed from the mass flow sensor. The valve allows thrusts ranging from 0 to 500 μN for both science and maneuver operations. The system is made fully redundant with two sets of 6 thrusters and two MPE. The two sets are located on three external panels, each one having a cluster of four thrusters, two from the prime sets or side-A and two from the redundant set or side-B.

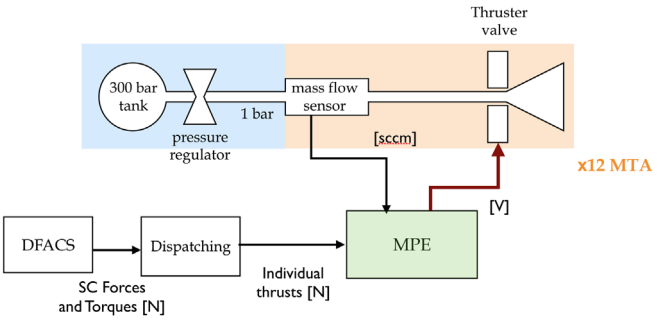

FIG. 1. Functional schematic of the full cold gas propulsion chain. For clarity reasons, only one microthruster assembly (MTA) and one feed line are represented. The *DFACS* is the controller that commands the forces and torques applied to the spacecraft. The dispatching converts spacecraft forces and torques into requested thrusts. The MPE is the electronic box that controls the MTA: mass flow sensors and piezo valve according to the requested thrust.

The satellite is controlled with six thrusters used simultaneously. The +z direction is defined as the direction normal to the solar panel. The attitude control during the science run forces the solar panel to face the sun so that the +z direction is in the sun pointing direction. All the thrusters have the same angle of ≈60 degree with respect to the sun and are all pointing opposite to it (see table I). Thus it is impossible with this thruster geometry to command a thrust in the −z direction. However, the solar radiation pressure (SRP) plus the outgoing infrared radiation exert a quasi constant force of the order of 25 μN, that can be considered as a 7th thruster in the −z direction. Note that this virtual 7th thruster has a constant thrust and so does not provide additional thrusts combination to generate a given spacecraft motion. Nonetheless, it allows the *DFACS* control algorithm to move the spacecraft in the −z direction despite the thrusters geometry. Figure 2 shows a view of the LISA Pathfinder S/C as seen from above and shows the orientation of the Z axis with respect to the solar panel.

This has two consequences for science operations:

(i) As the thrusters of a given set are operated at almost the same amplitudes, close to ∼9 μN, the impact of cross-talk effects between the thrusters can be neglected.
(ii) As the illumination of the spacecraft is quite constant, temperature variations are not expected to impact the gas system.

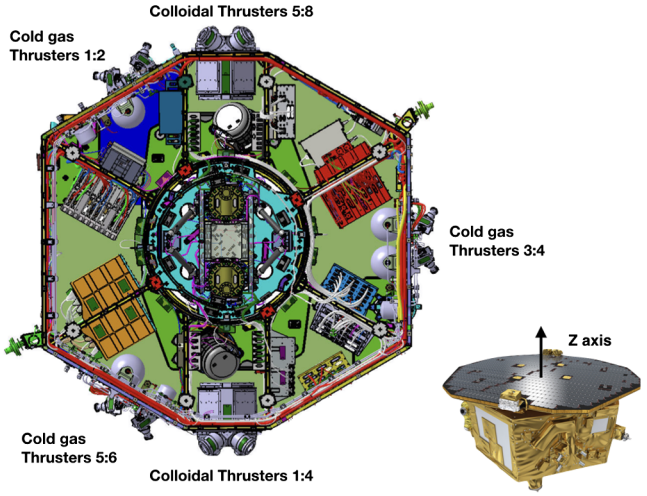

FIG. 2. A view of the LISA Pathfinder SC with the solar panel removed. The thrusters can be observed on the outside panels. The small view on the right side shows the orientation of the Z axis. The colloidal thrusters are on the top and bottom panels.

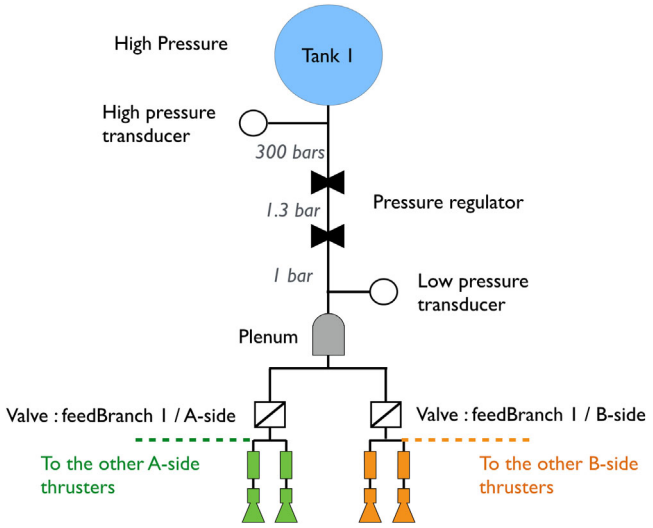

FIG. 3. Schematic of a panel with a propulsion system attached. Each of these panels has one N_2 feed line and four microthrusters, two from the prime A-side and two from the redundant B-side. One feed line can provide N_2 either to the A-side or B-side thrusters set by opening or closing the low pressure valve. The low pressure part of the feed line is pressure regulated to maintain a constant calibrated thrust.

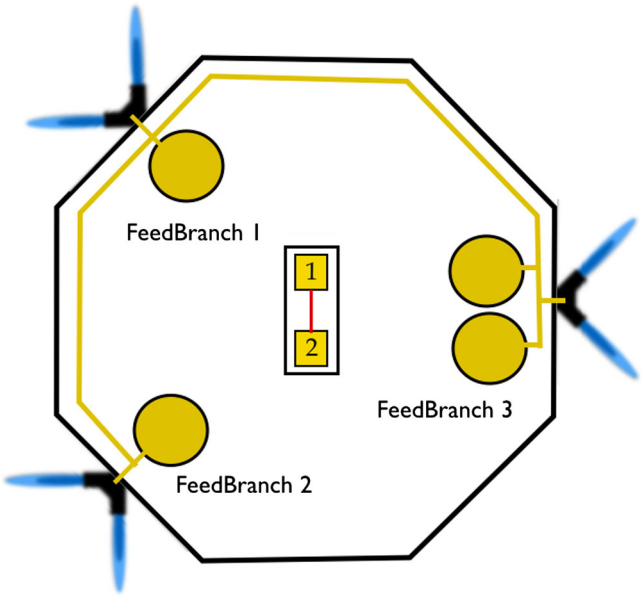

FIG. 4. Simplified sketch of the cold gas high pressure tank locations and feed branches of LISA Pathfinder. The two test masses are shown at the center of the spacecraft.

The feeding system is separated into a high pressure part where the N_2 gas is loaded to a pressure of 292 bars at the start of the mission and a low pressure part at 1 bar from which the thrusters are fed (see Fig. 3). While the high pressure part keeps decreasing during the mission due to propellant consumption, the low pressure side is maintained at a constant pressure by two pressure regulators. The stability of the low pressure is required for stable thruster operations. There are four high pressure tanks located at three extremities of the spacecraft (see Fig. 4), each extremity defining an independent feed line. Feed line one and two have their own high pressure tank while the third feed line has two tanks clustered together. A single feed branch—including both the high and low pressure plumbing illustrated in Fig. 3—is used by all 6 A (or B) thrusters, such that only a single tank is depleted at a time.

This propellant storage strategy has two objectives:

(i) Redundancy, in case of failure of one of the 3 independent high pressure feed lines.
(ii) Enough flexibility to have a dedicated tank emptying strategy to gravitationally balance the remaining fuel mass [9].

The propellant mass for the whole mission is about 10 kg which is ∼2% of the total mass of the satellite. After 9 months of operations ∼3 kg were spent, which means that the spacecraft is losing an average 10 g of mass per day. This mass loss directly modifies the gravity imbalance seen by the two test masses and its impact was calculated and included in the quasi DC drift of the differential acceleration (Δg) between the two test masses. This effect is observed at first order below 10^{-5} Hz so outside of the nominal measurement bandwidth, but still needs to be compensated by the tank emptying strategy to maintain a small differential gravitational field.

The functionality checks conducted during commissioning such as switching between feed lines or handling low and high simultaneous thrusts were successfully validated.

III. THRUSTER CHARACTERIZATION

A. Using commanded thrusts as a perturbation measurement

During the science operation, the thrusters are actuators in the multiple drag free control loops. As a consequence, their noise is not a directly measurable quantity. The first step is to estimate external perturbations on the spacecraft acceleration G_{SC_i}, the thrusters noise being one of them. For instance let us consider the sensitive axis x:

$$G_{SC_x} = -\frac{F_{cmd_x}}{M_{SC}} + \ddot{x_1} + \omega_1^2 \cdot x_1$$

Where x_1 is the measurement of the sensor used to control the spacecraft in x, ω_1^2 is a stiffness term, $\frac{F_{cmd_x}}{M_{SC}}$ is the total commanded thrusts in x divided by the spacecraft mass, and G_{SC_x} is any potential external disturbances along x. The commanded forces sent by the drag free algorithm (*DFACS*) to the thrusters (i.e., F_{cmd_x}) can be used to measure the spacecraft disturbances under two conditions:

(i) The controller open loop gain is very high so that both $x_1 \to 0$ and $\ddot{x_1} \to 0$.
(ii) When the loop gain is very high, commanded forces will also null-out the noise of the sensor

used in the loop. So sensing noises have to be low enough compared to any other disturbances (i.e., $\ddot{x}_{1_{\text{noise}}} \ll G_{SC_x}$).

Both conditions are met for the LISA Pathfinder within the bandwidth 0.1–10 mHz. The drag free loop counters the external noises effectively up to 100 mHz. The sensing noises have been estimated, approximately, at 35×10^{-15} mHz$^{-1/2}$ for the x interferometric position measurement, 2 nmHz$^{-1/2}$, for y and z capacitive measurements and 10^{-7} radHz$^{-1/2}$ for θ_1 capacitive measurement, see references [1] and [10]. Their impact on the spacecraft acceleration is well below the thrusters noise. Note that it also means that TMs are considered as perfect inertia reference frames for this study.

B. Thruster noise and other external perturbations

Among the disturbances modeled in the ∼mHz range on the spacecraft, a thruster noise of 0.1 μNHz$^{-1/2}$ is the dominant one and is at least an order of magnitude above the solar wind protons and the solar radiation pressure fluctuations impact on the spacecraft motion. These quantities have been estimated from ACE ([11]) measurements and projected on LPF. Still, it is not possible to disentangle in the commanded thrusts, the thrusters noise contribution from a potential unknown noise source. So complementary measurements were performed to understand this level of noise. As one of NASA's contributions, LISA Pathfinder included a second set of thrusters, i.e., the *colloidal thrusters* [12], they have been used to remove this ambiguity. The commanded forces on the Z axis of the spacecraft with similar control scheme but with three different thrusters configurations (i.e., facing the same amplitude of the SRP) have been compared (see Fig. 5):

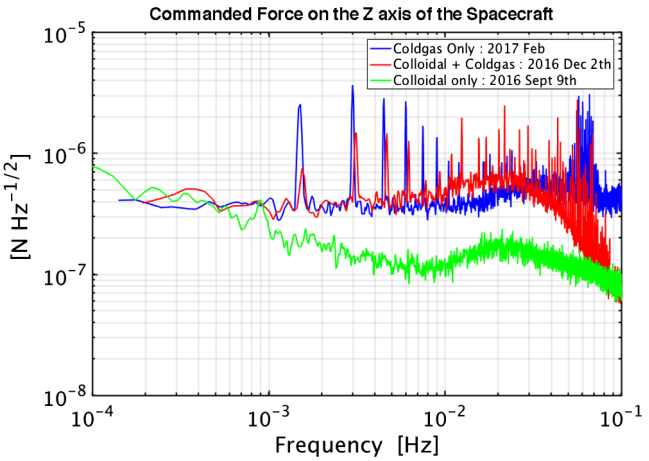

FIG. 5. Amplitude spectral density of commanded forces on the Z-axis of the spacecraft. The drag free is active in the three configurations. In green: Colloidal thrusters only are used. In red the colloidal thrusters are used for the drag free and an open loop thrusts is commanded on four cold gas thrusters. In blue, the cold gas thrusters only are used.

(1) The colloidal thrusters only are used for the drag free and solar radiation pressure (SRP) compensation (green line).
(2) The colloidal thrusters are used for the drag free but the SRP is partially compensated by an open loop force commanded on four cold gas thrusters (red line). Cold gas thrusters number 1,2, 5, and 6 have been used for this, with thrusts of 18.4, 12.5, 5.3, and 11 μN, respectively. The remaining 2 cold gas thrusters were set to provide 0 thrust, i.e., their noise contribution were not suppressed.
(3) The cold gas thrusters only are used for drag free and SRP compensation (blue line).

When the colloidal thrusters only are used, the noise associated with the force compensation applied to the spacecraft (green line in the figure) is four times lower at 10 mHz than in the two other configurations. In the second configuration, an additional open loop thrust on four of the cold gas thrusters was sufficient to increase the commanded force noise up to 0.4 μNHz$^{-1/2}$. This is exactly the noise level of the third configuration when the cold gas thrusters only are used for drag free operations. These measurements showed that cold gas thrusters noise are indeed the dominant source of external perturbation. As a consequence we can infer the level of noise of the cold gas thrusters by directly using the commanded thrusts.

C. Thruster noise general considerations

The six degrees of freedom of the spacecraft $(x_{SC}, y_{SC}, z_{SC}, \theta_{SC}, \eta_{SC}, \Phi_{SC})$ are controlled with six thrusters. As a consequence there is only one set of commanded thrusts that can achieve a given spacecraft motion. Moreover all these axis are drag free controlled with closed loop transfer functions equal to one up to 10 mHz [13]. Two major sources of correlations in the commanded thrusts unrelated to the thrusters were investigated:

(i) To constantly point toward the sun and keep the antenna oriented toward earth, it is necessary to apply additional torques on the spacecraft at low frequencies (below 0.5 mHz) referred as the attitude control. These torques could create a correlated signal between commanded thrusts that does not relate to the thruster noise. They were measured using the forces applied on the y/z axis of the TMs and are orders of magnitude lower than the measured commanded torques in the 0.02—10 mHz frequency band.
(2) The scheme by which the *DFACS* commands forces and torques to counter the movement of the spacecraft is followed by a *dispatching algorithm* (i.e., a distribution of the thrusts among the thrusters in order to apply the requested forces and torques to the spacecraft) that can be suspected to introduce a level of correlation between the thrusters. A study of such correlations has been performed using ESA's LISA

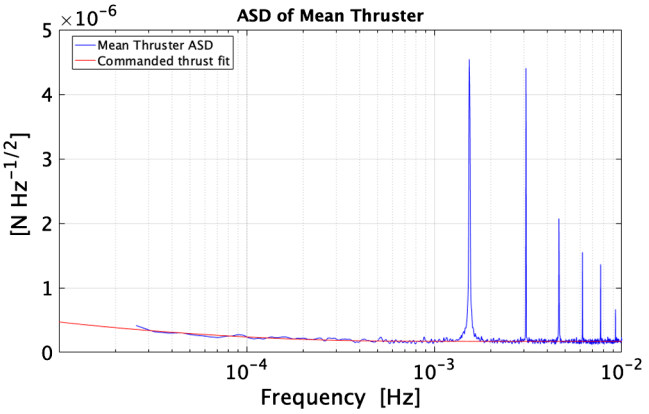

FIG. 6. Averaged commanded thrust amplitude spectral density (ASD) during a "noise" run (*DoY 95:104*) below 10 mHz where the commanded thrust noise is dominant. Below 0.3 mHz, the impact of the rotation of the spacecraft is observed, see Fig. 9. Above, a white noise behavior is observed with the presence of discreet lines.

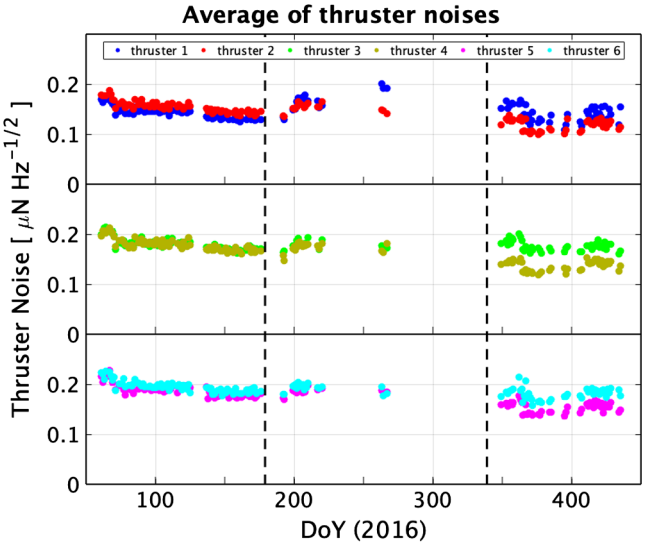

FIG. 7. Evolution of the average amplitude spectral density of each commanded thruster noises in the 1.7–2.7 mHz frequency range as a function of time (*DoY*). The three panels show, from top to bottom, thrusters 1–2, 3–4 and 5–6. The dashed lines indicate the period during which NASA's colloidal thrusters were used.

Pathfinder simulator which includes both the *DFACS* and the dispatching. The results show that no significant level of correlation is observed below 10 mHz and that, above, the correlations observed are explained by the impact of the *DFACS*.

So we expect the noise level of a given thruster, below 10 mHz, to be reflected as a noisy command of this particular thruster. Figure 6 shows the mean amplitude spectrum density, averaged over all 6 thrusters, of the commanded thrust during a science run (*DoY 95:104*). A few remarks can be made:

(i) The thrusters were calibrated during *Station Keeping* by the ESA Mission Operation Center in Darmstadt. It is estimated to be precise to better than 10%. That sets our major source of error when estimating thrusters noise.

(ii) Above 10 mHz the measured thruster noise increases due to the TM 1θ inertia sensor noise. This channel is used to control the Θ_{SC} axis (rotation around the sensitive axis).

(iii) Discrete lines are present at 1.5 mHz and its harmonics. Groups of lines are also present around 55 and 70 mHz. This will be discussed later in this section.

(iv) Below 0.3 mHz, the rise in amplitude is attributed to the rotation of the spacecraft, see Fig. 9.

(v) Discarding the observed lines, the noise between $0.3mHz$ and 10 mHz is constant with an average value of 0.17 $\mu\mathrm{N}/\sqrt{\mathrm{Hz}}$.

Figure 7 shows the evolution, over most of the mission, of the noise for each individual thruster between 1 and 10 mHz, after removal of the spectral lines (see Fig. 6). Each data point corresponds to a 24h measurement and their statistical errors are smaller than the size of the data points. Up to *DoY*272 set A thrusters were used and beyond there was a switch to set B. The black dotted lines, at *DoY*179 and 339, define the period when NASA's colloidal thrusters were used and which induced a significant increase (a few degrees) in the temperature of the S/C. This is a possible explanation for the increase of the noise in this period. Otherwise, the noise levels display rather stable values up to *DoY*179. Beyond *DoY*272, when set B thrusters were used and large temperature variations were imposed on the S/C, slightly larger fluctuations are observed.

The thrusters noise exceeds the mission requirements by around 70% but it still fits within the noise margin and does not impact the performances of LISA Pathfinder or of LISA. It will be seen, in the next section, that part of this noise is a *common (coherent) noise* which will need further ground studies to elucidate.

Prior to the mission, ground characterizations were performed [14] on a thruster flight model but without the feeding system and only down to 2 mHz because of test bench limitations. These tests demonstrated a noise lower than 0.1 $\mu\mathrm{NHz}^{-1/2}$ for similar range of thrusts, thus below the values observed in flight. This seems to imply a problem related with the feeding system common to both primary and redundant set of thrusters, even though, so far, no explicit investigation has demonstrated this.

D. Common (coherent) noise between thrusters

Figure 8 shows the amplitude spectral density (ASD) of the forces on the X, Y, and Z axis during a noise run. One observes that the noise level on the Z axis around 1 mHz is

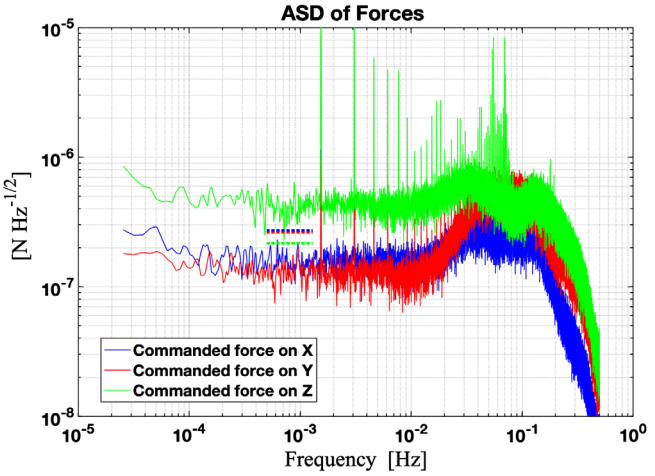

FIG. 8. Amplitude spectral density (ASD) of commanded forces for *DoY 95:104*. The dotted lines indicates the expected levels if the individual measured thruster noises were statistically incoherent.

significantly larger than those on the other axis. The dotted lines indicate the levels expected, around 1 mHz, if the thrusters noise measured by the individual thrusts commanded are projected on the X, Y, and Z and considered as statistically independent noises. The mismatch between expected and measured values and that these lines are also above the measured X and Y forces, can be explained by the presence of a *common noise*. Because of the orientations of the thrusters (see Table I), a *common noise* would *add up* on the Z axis whereas it would have a null impact on the X and Y axis where the sum of the direction cosines is quasinull. This asymmetry is observed in Fig. 8. Figure 9 shows the amplitude spectral density (ASD) of the torques around the X, Y, and Z axis during the same period and the

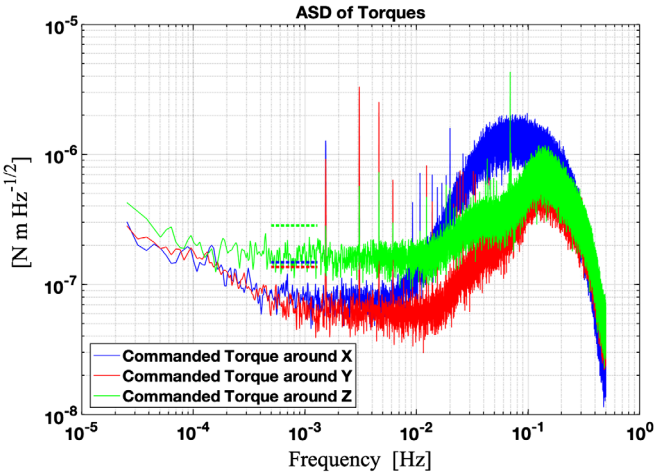

FIG. 9. Amplitude spectral density (ASD) of commanded torques for *DoY 95:104*. The dotted lines indicates the expected levels if the individual measured thruster noises were statistically incoherent.

projection of measured thrusters noise as incoherent noises. The difference between these predictions and the measurements can, there again, be explained by the orientation of the thrusters (see Table I) and the presence of a *common noise*. In order to evaluate the hypothesis of a *common noise*, a *coherence* analysis of the thruster noises has been performed.

Figure 10 shows the correlation values observed between thrusters 1 and 2 (red line) and between thrusters 5 and 6 (blue line), for *DoY 95:104* in both cases. Below 10 mHz a strong degree of correlation is observed. At the frequencies corresponding to the observed lines in Fig. 8 the correlation is 100%, as discussed in the preceding section, these lines are common to all thrusters. Apart from these discrete cases, the correlation stays close to 90% for the first case and close to 50% for the second. This indicates that there exists a common component between thrusters. The same observation can be made for all other thruster pairs (the coherence levels varying between 90% and 50%) and for the duration of the mission although a significant decrease of coherence is observed for *DoY* $\gtrapprox$300.

The method to extract this common noise component is the following:

(i) Figure 5 shows that the *common noise* measured on the Z-axis is independent of the average commanded thrusts (between 0 and 18.4 μN for the joint experiment with the colloidal or all thrusters at 9 μN for cold gas only) but inherent to the cold gas micropropulsion system. So the (strong) assumption is made that the common noise is equal on all thrusters, i.e., the level of common noise on thruster$_i$ (in μN/Hz) is the same as on thruster$_j$.

(ii) Using a coherence algorithm for each pair of thrusters that estimates the cross power spectrum between two time series, the level of the common component is extracted. There are therefore 15 such values from as many pairs.

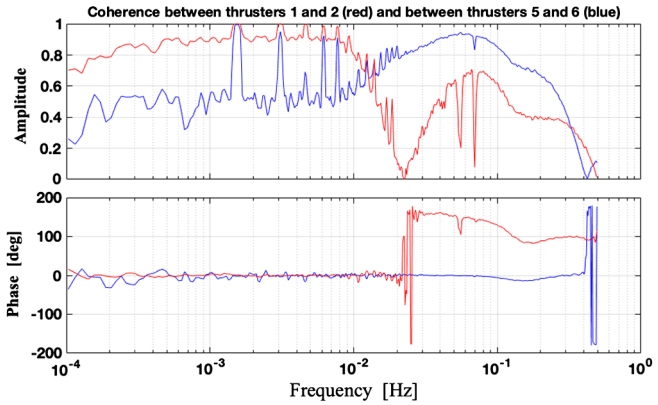

FIG. 10. Correlation (absolute value and phase difference) between thrusters 1 and 2 (red lines) and between thrusters 5 and 6 (blue lines) as measured during *DoY 95:104*. Above 10 mHz, the correlations are due to the DFACS system.

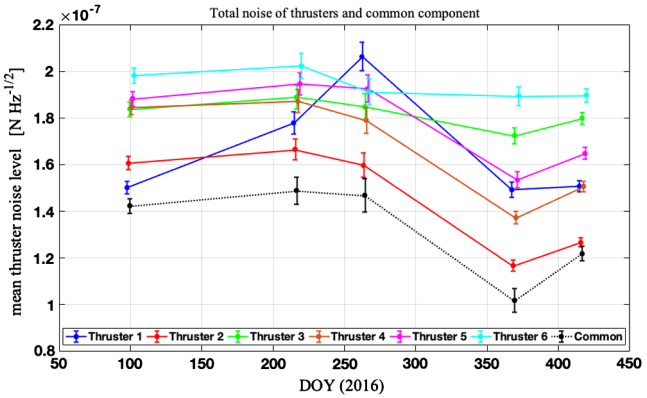

FIG. 11. Mean thruster noise as a function of *DoY*. The black dots indicate the average value of the common (coherent) part of the thrust, calculated between all possible pairs.

(iii) The average of these values is then used to estimate the common component. Taking the minimum of these values would diminish this estimate by only 10%.

Figure 11 displays, for each thruster, the mean noise level (in μNHz) during the whole mission after the impact of the spectral lines has been removed. These values are quite stable although some evolution is seen beyond *DoY 300*. The black points and dotted line shows the average *common (coherent) noise* over all thruster pairs and for each measurement using the method outlined above.

Figure 12 displays the level of uncorrelated thrust (in μNHz) for each thruster. The *uncorrelated noise* level is calculated by subtracting, in power, the *common noise* level from the total power. From this study, it is concluded that the uncorrelated (statistically independent) thruster noise of the thrusters can be estimated, in the mHz range, as a white noise with levels between 0.5 and 0.15 μN/Hz. The value for thruster 1 at *DoY 90* appearing as an outlier. The uncorrelated noise levels appear to be stable in time with an average level of ~0.10 μN/Hz, suggesting that the evolution of the total noise level beyond *DoY 300* (see figure 11) could be due to the evolution of the *common* noise contribution.

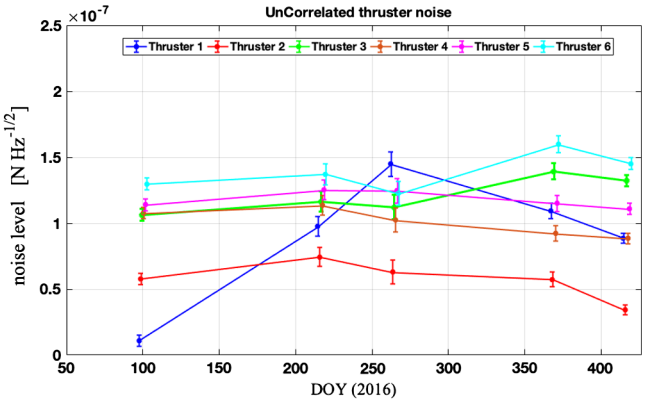

FIG. 12. Extracted uncorrelated thruster noises as a function of *DoY*. See text for further details.

E. Thrusters lines

As can be seen on Fig. 6, a number of discrete lines are observed at 1.5 mHz and its multiples. Other sets of lines are seen around 55 and 70 mHz. In fact all these lines appear to originate from the same source and, as shown above, are a feature of the cold gas propulsion system and 100% correlated between individual thrusts. The lines observed at 55 and 70 mHz are, as shown by Figs. 13 and 14, multiple lines separated by 1.5 mHz indicating that they probably have a common origin to the lines observed at lower frequencies.

The observation that these lines are extremely narrow seems to point to an electronic effect. As an example, a quality factor (QF $= f/\Delta f(@3db)$) of ~2000 is measured for the 3 mHz line during *DoY 95:104*.

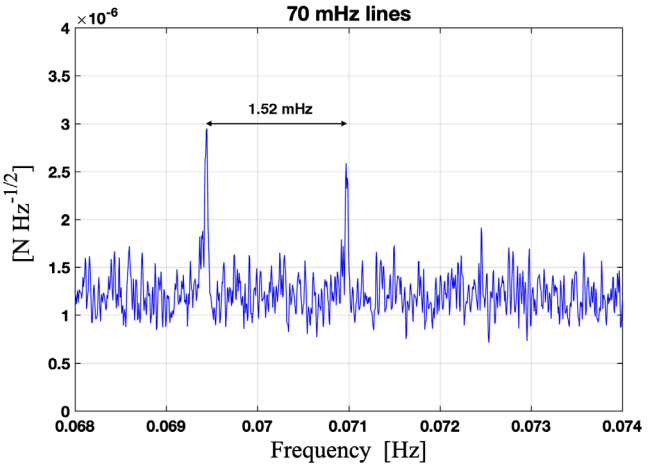

FIG. 13. Observed lines around 70 mHz. The lines are separated by 1.52 mHz. The lowest frequency line is observed at 1.54 mHz. Data for *DoY 95:104*.

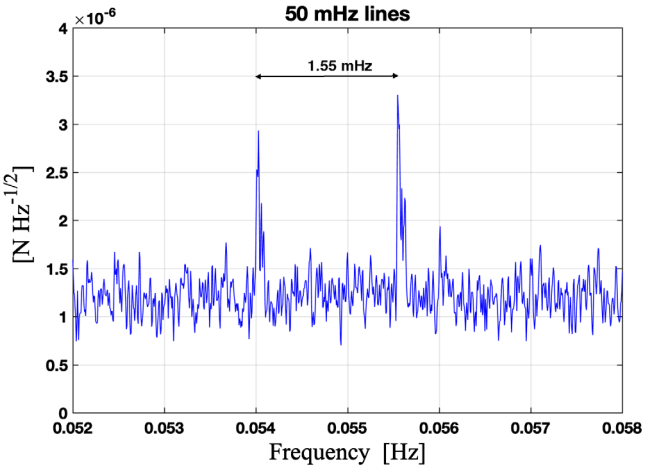

FIG. 14. Observed lines around 50 mHz. The lines are separated by 1.55 mHz The lowest frequency line is observed at 1.54 mHz. Data for *DoY 95:104*.

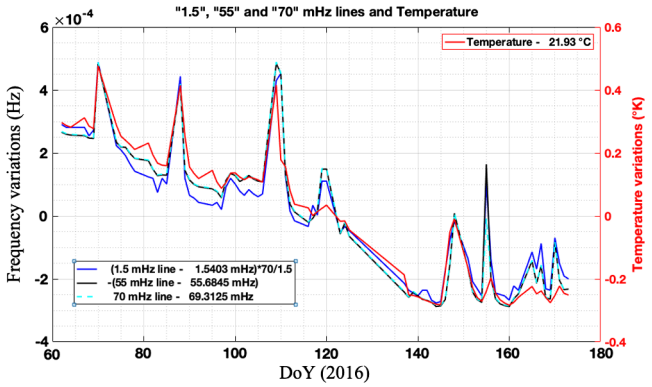

FIG. 15. Frequency evolution of 1.5, 55 and 70 mHz thruster lines during the mission and the average temperature of the satellite as a function of *DoY*. A strong correlation is seen with a coefficient of 0.02 mHz/K for the 1.5 mHz line.

It should be noted that they produce a real motion of the spacecraft since they can be seen by measurements of the distance between TM_1 and the spacecraft.

We are currently investigating a clock synchronization problem between the thruster electronic that runs a loop at 40 Hz and the *DFACS* that request commanded thrusts at $10Hz$ based on a separate clock. This seems to be confirmed by a study of their behavior during the mission that shows a correlation between the frequency of the lines and the average temperature of the spacecraft (see Fig. 15) with a coupling coefficient of 0.02 mHz/K for the line at 1.5 mHz. Further studies should be performed on a dedicated ground based test bed in order to track and eventually confirm their origin. It may be interesting to note that the line seen at 70 mHz shows a similar dependence upon temperature (but with a slope of 0.93 mHz/K) whereas the 55 mHz line has the same slope as the 70 mHz line but with a negative value (see Fig. 15). It is worth noting that the temperature dependence df/dT of the 70 mHz line is equal to 70/1.5 times the df/dT of the 1.5 mHz line.

IV. PROJECTION FOR LISA

Even though greatly reduced by the drag free controller, the thrusters noise is an important source of spacecraft motion with respect to the test masses above ~mHz [13]. Measurements of the thrusters induced motion are given on LPF by in-loop drag free controlled channels: x_1, $y_1 + y_2$, $z_1 + z_2$, $y_1 - y_2$, $z_1 - z_2$, and θ_1. The motion itself does not directly couple with the test mass to test mass measurement error. In LPF, the optical bench or spacecraft motion is correlated between the two TMs so that it is eliminated when the differential acceleration (Δg) is computed. For LISA, the optical bench displacement noise will also be completely suppressed after reconstruction of the test mass-test mass measurement between two satellites with the time delay interferometry algorithm. However, thruster noises, through spacecraft motion, will impact LISA via two main physical effects:

(i) Optical imperfections (misalignments and wavefront error) will couple spacecraft motion into optical path length error. This source of noise is usually referred to as tilt to length coupling (TTL) for the spacecraft angular jitter coupling.

(ii) A moving spacecraft will couple the TM-spacecraft relative position with any gradient field such as the spacecraft self-gravity or the electrostatic field. This coupling generates a parasitic force on the TM proportional at the first order with the TM position (i.e., a stiffness term).

Both these effects were characterized on LPF but will impact LISA differently. In LPF the test masses are affected by the same spacecraft motion, so a significant part of the stiffness noises contribution appeared as correlated noise and vanished when computing Δg. The stiffness coefficient was measured via dedicated experiments at $\omega_1^2 = (-525 \pm 30) \times 10^{-9}/s^2$ while differential stiffness ($\Delta\omega_{12}^2$) was consistent with zero [1]. For LISA, spacecraft motion will be uncorrelated between two distant spacecraft so that contributions for a test mass to test mass measurement will be incoherent and sum up quadratically in the noise budget. If we assume similar levels of stiffness and design of drag free controller, the expression $\sqrt{2} \cdot x1 \cdot \omega_1^2$ gives a rough estimation of the thrusters impact on stiffness noise for LISA. The additional factor of $\sqrt{2}$ is applied to take into account the effect on both test masses. This contribution has a maximum of 6.7×10^{-15} ms^{-2} at 25 mHz which is well below the LISA noise curve requirement in terms of differential acceleration as shown in [1].

In LPF spacecraft pickup into Δg was mainly due to misalignment between the TMs, the GRS and the spacecraft. The resulting contribution appeared as a *bump* between 20 mHz and 100 mHz. It was subtracted by fitting a simple model using other TM's degrees of Freedom measurements [8]. The optical layout in LISA to do a test mass to test mass measurement is much more complex as it involves multiple interferometers and imaging systems. More sources of misalignment as well as the wavefront error of the transmitted beam will greatly increase the level of coupling between angular or lateral jitter of the spacecraft and the main measurement. Postprocessing subtraction of this noise will be mandatory to achieve the required performance for LISA. The subtraction method will not be as straightforward as for LPF since it will rely on the time delay interferometry algorithm first to reconstruct laser noise free signals. So, minimizing the thrusters noise impact on the spacecraft jitter by DFACS design or by a better handling of the common noise and lines will be crucial for this source of noise.

V. CONCLUSION

The full cold gas propulsion system (i.e., the thrusters with their feeding system) was characterized with a flat

white noise component of $\sim 0.17\ \mu\mathrm{N}/\mathrm{Hz}$ down to 0.02 mHz. This noise has been decomposed into a common (coherent) and incoherent part, both of comparable amplitudes. The presence of lines and the common (coherent) part of the noise were identified as a cold gas thruster system contribution by joint use of the NASA provided colloidal propulsion system with the cold gas system.

As there is no clear evidence on the origin of these artefacts, the observations that have been made in-flight (correlation of the lines with the temperature, a noise insensitive to the thrusters used) should lead to specific ground experiments in order to elucidate and remedy these effects.

The gain of the thrusters were calibrated by ESA's Mission Operation Center during station keeping and the values obtained seem reliable to better than 10%.

For LISA, the gain fluctuation have no consequences on its predicted performances. However, the observed spectral lines and the excess coherent noise will induce spacecraft motion that will couple with the test masses sensitive axis motion through stiffness and optical imperfections. Their expected level could be non-negligible. Dedicated studies or design strategy should therefore be devoted to explain or suppress their presence.

ACKNOWLEDGMENTS

This work has been made possible by the LISA Pathfinder mission, which is part of the space-science programme of the European Space Agency. The French contribution has been supported by the CNES (Accord Specifique de projet CNES 1316634/CNRS 103747), the CNRS, the Observatoire de Paris and the University Paris-Diderot. E. Plagnol and H. Inchauspé would also like to acknowledge the financial support of the UnivEarthS Labex program at Sorbonne Paris Cité (ANR-10-LABX-0023 and ANR-11-IDEX-0005-02). The Albert-Einstein-Institut acknowledges the support of the German Space Agency, DLR. The work is supported by the Federal Ministry for Economic Affairs and Energy based on a resolution of the German Bundestag (FKZ 50OQ0501 and FKZ 50OQ1601). The Italian contribution has been supported by Agenzia Spaziale Italiana and Istituto Nazionale di Fisica Nucleare. The Spanish contribution has been supported by contracts AYA2010-15709 (MICINN), ESP2013-47637-P, and ESP2015-67234-P (MINECO). M. Nofrarias acknowledges support from Fundacion General CSIC (Programa ComFuturo). F. Rivas acknowledges an FPI contract (MINECO). The Swiss contribution acknowledges the support of the Swiss Space Office (SSO) via the PRODEX Programme of ESA. L. Ferraioli is supported by the Swiss National Science Foundation. The UK groups wish to acknowledge support from the United Kingdom Space Agency (UKSA), the University of Glasgow, the University of Birmingham, Imperial College, and the Scottish Universities Physics Alliance (SUPA). J. I. Thorpe and J. Slutsky acknowledge the support of the U.S. National Aeronautics and Space Administration (NASA).

[1] M. Armano *et al.*, Phys. Rev. Lett. **116**, 231101 (2016).
[2] P. A. Seoane *et al.* (The eLISA Consortium), arXiv:1305.5720.
[3] M. Armano *et al.*, Phys. Rev. Lett. **120**, 061101 (2018).
[4] G. Morris, N. Dunbar, P. Bianco, and C. Edwards, in *49th AIAA/ASME/SAE/ASEE Joint Propulsion Conference, Design of a Cold-Gas Micropropulsion system for LISA Pathfinder, San Jose, California, USA, 2013* (2013), https://doi.org/10.2514/6.2013-3854.
[5] G. Noci, G. Matticari, P. Siciliano, L. Fallerini, L. Boschini, and V. Vettorello, in 45th AIAA/ASME/SAE/ASEE Joint Propulsion Conference and Exhibit, Cold Gas Micro Propulsion System for Scientific Satellite Fine Pointing: Review of Development and Qualification Activities, Thales Alenia Space Italia, Denver, Colorado, USA, 2009 (2009), https://doi.org/10.2514/6.2009-5127.
[6] A. Polli, in 65th International Astronautical Congress 2014, Space Propulsion Symposium (C4), European Cold Gas Micro Propulsions System reached TRL-9 on board GAIA S/C. Discussion on in Flight Performance and System Flexibility and Capabilities for Being Implemented in other Mission Requiring Ultra-Fins Satellite Positioning and Attitude, Propulsion Technology (1) (3), Toronto, Canada, 2014 (2014), https://iafastro.directory/iac/paper/id/26175/summary/.
[7] A. Schleicher, T. Ziegler, R. Schubert, N. Brandt, P. Bergner, U. Johann, W. Fichter, and J. Grzymisch, CEAS Space J. **10**, 471 (2010).
[8] M. Armano *et al.*, Phys. Rev. D **97**, 122002 (2018).
[9] M. Armano *et al.*, Classical Quantum Gravity **33**, 235015 (2016).
[10] M. Armano *et al.* (LISA Pathfinder Collaboration), Phys. Rev. D **96**, 062004 (2017).
[11] D. McComas, S. Bame, P. Barker, W. Feldman, J. Phillips, P. Riley, and J. Griffee, Space Sci. Rev. **86**, 563 (1998).
[12] G. Anderson, J. Anderson, M. Anderson, G. Aveni, D. Bame, P. Barela, K. Blackman, A. Carmain, L. Chen, M. Cherng *et al.*, Phys. Rev. D **98**, 102005 (2018).
[13] M. Armano *et al.*, Phys. Rev. D **99**, 082001 (2019).
[14] J. Jarrige, P. Thobois, C. Blanchard, P.-Q. Elias, D. Packan, L. Fallerini, and G. Noci, J. Propul. Power **30**, 934 (2014).